Kobe University Repository : Kernel

PDF issue: 2025-12-05

Line shape engineering of sharp Fano resonance in Al-based metal-dielectric multilayer structure

Hayashi, S. ; Fujiwara, Y. ; Kang, B. ; Fujii, M. ; Nesterenko, D. V. ; Sekkat, Z.

(Citation)
Journal of Applied Physics,122(16):163103-163103

(Issue Date)
2017-10-28

(Resource Type)
journal article

(Version)
Version of Record

(Rights)
©2017 AIP Publishing. This article may be downloaded for personal use only. Any other use requires prior permission of the author and AIP Publishing. The following article appeared in Journal of Applied Physics 122(16), 163103 and may be found at http://dx.doi.org/10.1063/1.5002715

(URL)
https://hdl.handle.net/20.500.14094/90004442

Line shape engineering of sharp Fano resonance in Al-based metal-dielectric multilayer structure

S. Hayashi, Y. Fujiwara, B. Kang, M. Fujii, D. V. Nesterenko, and Z. Sekkat

Citation: Journal of Applied Physics **122**, 163103 (2017);
View online: https://doi.org/10.1063/1.5002715
View Table of Contents: http://aip.scitation.org/toc/jap/122/16
Published by the American Institute of Physics

Articles you may be interested in

Thermochromic VO_2 thin films on ITO-coated glass substrates for broadband high absorption at infra-red frequencies
Journal of Applied Physics **122**, 163107 (2017); 10.1063/1.5008730

Optoelectronics of inverted type-I CdS/CdSe core/crown quantum ring
Journal of Applied Physics **122**, 163102 (2017); 10.1063/1.4986638

A semi-analytical model of a near-field optical trapping potential well
Journal of Applied Physics **122**, 163101 (2017); 10.1063/1.5000269

A three-dimensional all-metal terahertz metamaterial perfect absorber
Applied Physics Letters **111**, 051101 (2017); 10.1063/1.4996897

Detection of guided-wave plasmon polariton modes in a high-index dielectric MIM structure
Journal of Applied Physics **122**, 123101 (2017); 10.1063/1.5001902

Clocking plasmon nanofocusing by THz near-field streaking
Applied Physics Letters **111**, 131102 (2017); 10.1063/1.4991860

JOURNAL OF APPLIED PHYSICS **122**, 163103 (2017)

Line shape engineering of sharp Fano resonance in Al-based metal-dielectric multilayer structure

S. Hayashi,[1,2,a)] Y. Fujiwara,[1] B. Kang,[1] M. Fujii,[1] D. V. Nesterenko,[3,4] and Z. Sekkat[2,5,6]
[1]*Department of Electrical and Electronic Engineering, Graduate School of Engineering, Kobe University, Kobe 657-8501, Japan*
[2]*Optics and Photonics Center, Moroccan Foundation for Science, Innovation and Research (MAScIR), Rabat 10100, Morocco*
[3]*IPSI RAS - Branch of the FSRC "Crystallography and Photonics" RAS, Samara 443001, Russia*
[4]*Faculty of Information Technology, Samara National Research University, Samara 443086, Russia*
[5]*Faculty of Sciences, University Mohamed V, Rabat 10010, Morocco*
[6]*Graduate School of Engineering, Osaka University, Suita 585-0871, Japan*

(Received 31 August 2017; accepted 9 October 2017; published online 23 October 2017)

A systematic experimental study was performed on the Fano line shape exhibited by multilayer structures consisting of an Al layer, a SiO_2 spacer layer, and an Al_2O_3 waveguide layer. In the structures studied, a sharp Fano resonance appears on the background of broad asymmetric resonance attributed to the excitation of a surface plasmon polariton at the Al/SiO_2 interface. It is shown that the background asymmetric surface plasmon resonance can be well fitted to a single Fano function, and the sharp Fano line shape can be well fitted to a double Fano function expressed as a product of two single Fano functions. The results of measurements performed by varying the spacer layer thickness indicate that the width (Q factor) of the sharp Fano resonance decreases (increases) monotonously as the thickness increases. The Q factor achieved in the present study is as high as $\sim$1500. A comparison with the results of electromagnetic calculations suggests that not only the spacer layer thickness but also the imaginary part of the dielectric constant of the waveguide layer plays an important role in the Fano line shape engineering. *Published by AIP Publishing.* https://doi.org/10.1063/1.5002715

I. INTRODUCTION

In the past decade, optical responses of a variety of plasmonic nanostructures and metamaterials have attracted considerable interest because they have potential applications in optical devices such as optical switches, sensors, and enhancers of Raman, fluorescence, and nonlinear optical signals.[1–5] Among others, Fano resonances arising from coupling between dark and bright modes have been the subject of extensive theoretical and experimental studies.[6–11] Metallic nanowire arrays,[12] clusters of nanoparticles,[13–17] disk/ring nanocavities,[18–20] and metal-insulator-metal waveguides coupled to resonators[21] are only a few examples of nanostructures that exhibit the Fano resonance. Although the observation of the Fano resonances in such nanostructures was successful, the nanofabrication of the structures is time consuming and of high cost, preventing real applications. The quest for simpler structures that do not require the use of nanofabrication still remains a challenge.

In our recent publications,[22–25] we have proposed, based on electromagnetic (EM) calculations, a very simple multilayer structure that exhibits a sharp Fano resonance in the angle-scan attenuated total reflection (ATR) spectra in the Kretschmann configuration. The structure proposed is a multilayer stack consisting of a metal layer and three dielectric layers attached to a prism. In this structure, a metal-dielectric interface that supports a surface plasmon polariton (SPP) mode is placed close to a system of three dielectric layers which supports a planar waveguide (PWG) mode; the SPP and PWG modes can interact with each other through the overlap of their evanescent near fields inside a spacer layer. The Fano resonance is thus generated by the interference of a broad SPP mode (bright mode) with a sharp PWG mode (dark mode). Preparing multilayer samples consisting of an Ag layer, a fluoropolymer Cytop spacer layer, and a poly (methyl methacrylate) (PMMA) waveguide layer, we have succeeded in experimentally observing the Fano line shape.[26] Furthermore, we have demonstrated the light-tuning of the Fano resonance using a PMMA waveguide layer doped with photofunctional molecules (disperse red 1).[27,28] Very recently, Zheng *et al.*[29] reported the results of experimental and numerical studies on the Fano resonance in a multilayer structure consisting of an Au layer, a SiO_2 layer, and a ZrO_2 layer surrounded by water.

Although the experimental studies mentioned above[26–29] demonstrated the feasibility of realizing the Fano resonance in the metal-insulator multilayer structure, the experimental work is still in its initial stage and no attempt has been reported to systematically control the Fano line shape. To achieve extremely high sensitivities for refractive index sensing and giant enhancements of the electric field predicted theoretically,[22–25] one has to know how to engineer the Fano line shape and optimize the structural parameters. According to our theoretical analyses,[22–24] the major parameters that control the Fano line shape are the thickness of the spacer layer, which governs the strength of coupling between

[a)]s.hayashi@dragon.kobe-u.ac.jp

the SPP and PWG modes, and the imaginary part of the dielectric constant of the waveguide layer, which is related to the loss of EM energy inside the waveguide. In a real waveguide layer, the estimation of the magnitude of the imaginary part of its dielectric constant is very important because our analyses suggest that the magnitude fixes the optimum values of the Q factor, figure of merit (FOM) of sensing sensitivity, and field enhancement factor (FEF). Zheng *et al.*[29] reported extremely high theoretical values of the Q factor and FOM of sensitivity based on EM calculations. However, their extremely high values are not realistic because in their calculations, they neglected the imaginary part of the dielectric constant of the ZrO_2 waveguide layer. To establish Fano line shape engineering, systematic experimental studies are still required to elucidate the roles played by the thickness of the spacer layer and the imaginary part of the dielectric constant of the waveguide layer.

To further explore the intriguing properties of the Fano resonance in the metal-dielectric multilayer structure and establish a way of engineering the Fano line shape, we performed a systematic experimental study of the Fano resonance in Al-based multilayer structures. The reasons why we chose Al are multiple. It is well known that in the visible spectral region, Al films exhibit SPP resonances much broader than those of Ag and Au films.[30,31] In plasmonics, normally sharper SPP resonances are required to obtain higher device performances. However, in our multilayer Fano structures, the broadness of the SPP resonance turns to be advantageous because it is not necessary to tune finely the sharp PWG resonance to the SPP resonance to assure their overlap and coupling. Furthermore, Al is a low cost material with well-known optical properties. In addition, as described in detail in recent review papers[32,33] and references cited therein, Al-based plasmonic structures are operational in the UV spectral region (UV plasmonics), where they have good plasmonic properties because of low losses in Al, which is not the case for Ag- and Au-based structures.

In this paper, we report the results of ATR measurements performed by varying the thickness of the spacer layer. The width of the Fano line shape and consequently the Q factor are shown to depend strongly on the thickness. A Q factor as high as ~1500 is demonstrated experimentally. In this work, the imaginary part of the dielectric constant of the waveguide layer is experimentally estimated. From a comparison with EM calculations, we demonstrate that the magnitude of the imaginary part plays an important role in determining the Fano line shape.

II. EXPERIMENTAL

The structure of samples prepared is schematically shown in Fig. 1(a). Figure 1(b) shows a typical cross-sectional image of a sample obtained by using a scanning electron microscope (SEM) (Hitachi S-3100). First, an Al layer was deposited on a cleaned SF11 glass substrate by a vacuum evaporation technique. Then, a SiO_2 layer and an Al_2O_3 layer were successively deposited on top of the Al layer using a rf magnetron sputtering technique. Targets of SiO_2 and Al_2O_3 four inches in diameter were mounted on an

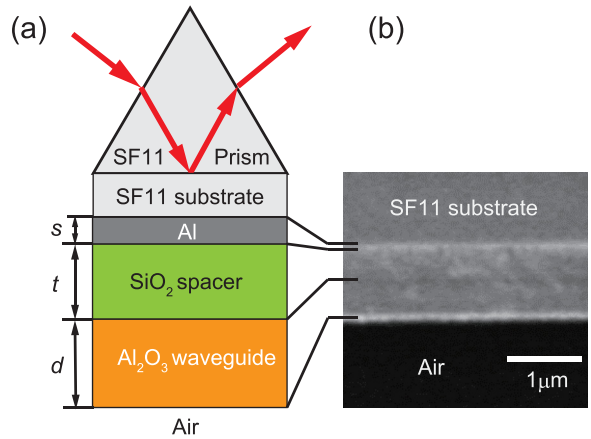

FIG. 1. (a) Structure of samples prepared. (b) Cross-sectional SEM image of a sample.

Anelva SPF210H sputtering apparatus and sputtered with a rf power of 200 W in an Ar gas of ~2.7 Pa. The thickness of the Al layer was monitored by a quartz microbalance during the deposition. The thicknesses of the SiO_2 and Al_2O_3 layers were controlled by choosing appropriate sputtering durations based on predetermined sputtering rates. For the SEM observation, the substrate with a stack of the layers was first broken to expose its cross section and dipped into a buffered HF etchant to slightly etch the SiO_2 layer. Then, the sample was coated by a thin Au layer to prevent the charge-up effects. The SEM image shown in Fig. 1(b) confirms the multilayer structure consisting of the Al, SiO_2, and Al_2O_3 layers deposited on the substrate. For comparison purposes, we also prepared reference samples, which have only the SiO_2 layer deposited on the Al layer.

To measure the ATR spectra in the Kretschmann configuration, the multilayer sample was pasted onto the bottom surface of a 60°-prism made of SF11 glass with the aid of index matching fluid. The prism with the sample was mounted on a computer-controlled $\theta - 2\theta$ rotating stage. p-polarized light from a He-Ne laser with a wavelength of 632.8 nm was incident on the prism through a chopper. The intensity of the reflected light was measured as a function of the angle of incidence, using a Si photo-diode connected to a lock-in-amplifier. The reflectance spectra were obtained by normalizing the intensity data recorded for the sample to those recorded for a bare substrate without the multilayer stack. The precision of the incident angle (internal angle inside the prism) in the present measurements is around 0.003°.

III. RESULTS AND DISCUSSION

A. Analysis of the observed Fano line shape

Typical ATR spectra obtained for the multilayer stacks without and with the Al_2O_3 waveguide layer are shown in Figs. 2(a) and 2(b), respectively. The spectrum obtained without the Al_2O_3 waveguide layer [Fig. 2(a)] exhibits a broad asymmetric ATR dip attributed to the excitation of the SPP mode at the Al/SiO_2 interface, in good agreement with previous ATR studies of Al films.[30,31] In the presence of the

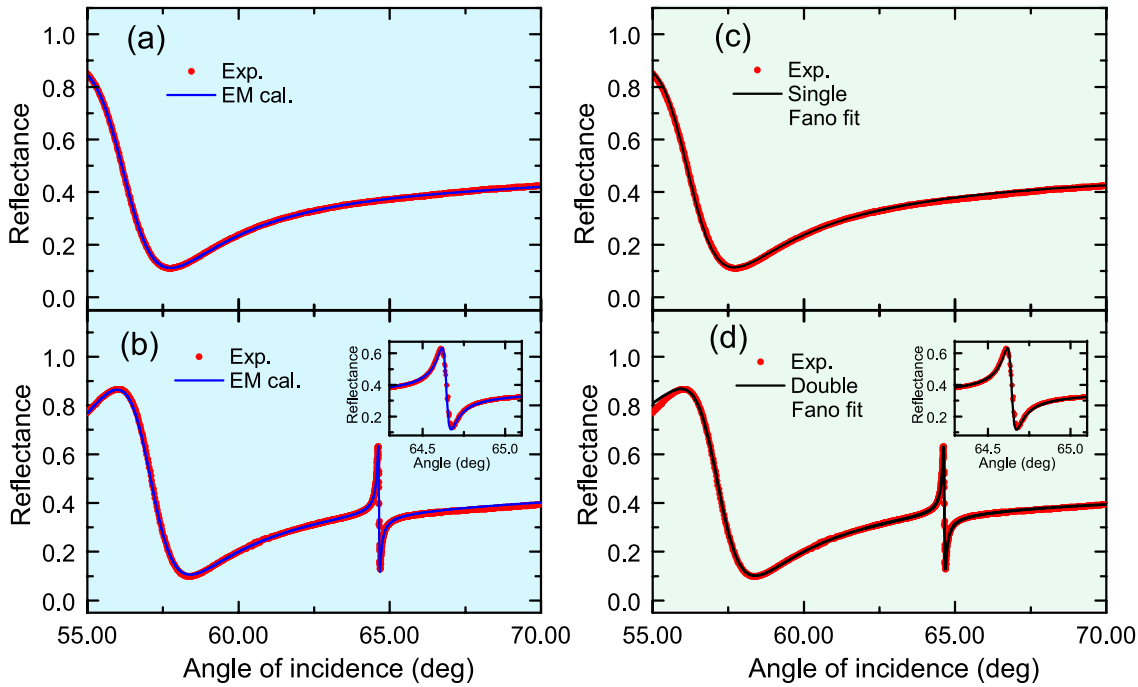

FIG. 2. (a) Experimental ATR spectrum of a sample without the Al_2O_3 waveguide layer and a fit curve obtained by an EM calculation. (b) Experimental ATR spectrum of a sample with an Al_2O_3 waveguide layer and an EM fit curve. (c) Experimental ATR spectrum identical to that shown in (a) and a result of fitting to the single Fano function. (d) Experimental ATR spectrum identical to that shown in (b) and a result of fitting to the double Fano function.

Al_2O_3 waveguide layer [Fig. 2(b)], a sharp Fano resonance appears around 64.7° in the tail region of the SPP dip. As discussed in detail in our previous papers,[22,23,26,27] this Fano resonance is caused by the coupling of the SPP mode localized at the Al/SiO_2 interface with the PWG mode supported by the Al_2O_3 waveguide layer. As we see in Fig. 2(a), the SPP resonance presently observed with the Al layer is very broad, extending from 57° to 70°. The resonance is almost twice as broad as those exhibited by Ag/dielectric and Au/dielectric interfaces in similar multilayer structures.[22,23,26,27] It should be noted here that the broad SPP resonance is advantageous in realizing the Fano resonance in our multilayer structures because it is not necessary to control precisely the thickness of the waveguide layer to tune finely the resonance angle of the sharp PWG mode into the SPP resonance to assure their overlap and coupling. Using the Al-based multilayer structure, we can generate the Fano resonance in a wide range of waveguide layer thicknesses, roughly twice as wide as those for Ag- and Au-based structures.

The solid lines in Figs. 2(a) and 2(b) represent the results of EM calculations performed by a freely available Winspall software package, which allows us to calculate ATR spectra by varying the structural parameters. We see that the experimental spectra are very well reproduced by the EM fit curves. In the fitting procedure, the dielectric constant of the SF11 prism was set to $\varepsilon_{SF11} = 3.163$.[34] The fit curve shown in Fig. 2(a) was obtained by a set of parameters: $s = 20.68$ nm and $\varepsilon_{Al} = -38.94 + i16.55$ for the Al layer and $t = 400$ nm and $\varepsilon_{SiO_2} = 2.126$ for the SiO_2 layer. The parameters for the fit curve of Fig. 2(b) are $s = 20.95$ nm and $\varepsilon_{Al} = -37.28 + i16.33$ for the Al layer, $t = 363$ nm and $\varepsilon_{SiO_2} = 2.124 + i2.915 \times 10^{-4}$ for the SiO_2 layer, and $d = 563$ nm and $\varepsilon_{Al_2O_3} = 2.788 + i3.673 \times 10^{-4}$ for the Al_2O_3 layer.

In the above fitting procedure, we did not take into account the existence of the oxide layer at the Al surface. However, it is known that when a vacuum evaporated Al film is exposed to laboratory air, a native oxide (Al_2O_3) layer a few nm in thickness is formed.[32,35] We checked the influence of the oxide layer on the fitting results and found the following facts. When an Al_2O_3 layer a few nm in thickness is inserted between the Al and SiO_2 layers in the EM calculations, only a portion of the ATR spectrum corresponding to the SPP resonance is appreciably modified, while that corresponding to the sharp Fano resonance remains almost the same. As a consequence, to obtain good fits to experimental results, mainly the parameters for the Al film have to be modified appreciably (up to ~10%), while the remaining parameters for the SiO_2 and Al_2O_3 layers have to be modified only slightly (less than a few percent). These results suggest that the parameters of the Al layers obtained without inserting the oxide layer are effective ones that reflect the effects of the surface oxide layer. For simplicity, throughout this work, we use the parameters obtained by neglecting the oxide layer. The overall good fits allow us to use these fitting parameters as good estimates of the thicknesses and dielectric constants of the layers in the present samples.

As evident from Fig. 2(a), the ATR dip corresponding to the SPP excitation at Al/SiO_2 is highly asymmetric. Although SPP dips observed for various metallic films were commonly analyzed using the Lorentzian line shape,[36,37] it is very much plausible that the SPP dip seen in Fig. 2(a) takes the Fano line shape. To check this point, we attempted to fit the observed line shape to a generalized function of the Fano line shape derived by Gallinet and Martin.[38,39] According to them, asymmetric line shapes of optical responses arising

from interferences between a nonradiative (dark) mode and a flat continuum of a radiative (bright) mode are given by

$$\sigma_a(\omega) = c\frac{\left(\frac{\omega^2-\omega_a^2}{2W_a\omega_a}+q\right)^2+b}{\left(\frac{\omega^2-\omega_a^2}{2W_a\omega_a}\right)^2+1}, \quad (1)$$

where ω_a and W_a are the resonance frequency and width, respectively, q is the Fano factor that governs the asymmetry, b is the modulation damping parameter, and c is the scale factor. The above line shape function is a generalization of the original Fano function[6,7,40] to the case where the dark mode resonance has intrinsic losses coming from the material losses, normally in metallic nanostructures. The effects of the losses are quantified by the parameter b. To apply the above generalized Fano function to our experimental data, the frequency ω has to be replaced by the angle of incidence θ. The result of fitting to the above generalized Fano function is presented in Fig. 2(c). The experimental data (dots) are the same as those presented in Fig. 2(a), and the solid line is the fit curve obtained by a set of parameters: $c = 0.504$, $\theta_a = 56.15°$, $W_a = 1.60°$, $q = -0.760$, and $b = 0.393$. In the present Fano line shape, the maximum is located at an angle lower than that of the minimum; in this case, the line shape can be fitted with a negative value of q. Figure 2(c) demonstrates that the experimental data can be fitted very well by the generalized Fano function. This implies that the SPP resonance can be regarded as the Fano resonance. To the best of the author's knowledge, the physical origin of the asymmetric line shape of the SPP dip has not been discussed in depth. In our group, analyses of the asymmetric SPP dips based on the EM theory and the coupled-mode theory are in progress, and the results will be published elsewhere.

In a variety of plasmonic nanostructures, the spectrum of the radiative (bright) mode is not flat and can be described by a symmetric Lorentzian line shape $\sigma_s(\omega)$. In analyzing asymmetric line shapes superposed on the symmetric Lorentzian line shape, Gallinet and Martin[39] introduced a total line shape $\sigma_t(\omega) = \sigma_s(\omega)\sigma_a(\omega)$, given by a product of the symmetric and asymmetric line shapes. They demonstrated that this expression of $\sigma_t(\omega)$ is very much successful to reproduce the Fano line shapes obtained by surface integral numerical simulations for a variety of nanostructures such as dolmen nanostructures, plasmonic quadramers and heptamers, and metallic photonic crystals.

As can be seen in Fig. 2(b), the presently observed sharp asymmetric Fano line shape is superposed on the broad asymmetric line shape, instead of a symmetric line shape. Therefore, to analyze the present sharp Fano line shape, it is natural to modify the total line shape function of Gallinet and Martin[39] and express it as a product of two asymmetric line shapes given by

$$\sigma_t(\theta) = \sigma_{a1}(\theta)\sigma_{a2}(\theta), \quad (2)$$

where $\sigma_{a1}(\theta)$ and $\sigma_{a2}(\theta)$ are the asymmetric line shapes given by Eq. (1) with two different sets of parameters, $c_i, \theta_{ai}, W_{ai}, q_i$, and b_i $(i = 1, 2)$. It is appropriate to call this line shape function as a double Fano function. In Fig. 2(d), a result of fitting of the experimental ATR spectrum to the double Fano function is presented. The experimental data (dots) are the same as those shown in Fig. 2(b). The fit curve was obtained by two sets of parameters: $c_1 = 0.461$, $\theta_{a1} = 57.11°$, $W_{a1} = 1.224°$, $q_1 = -0.826$, and $b_1 = 0.410$ for $\sigma_{a1}(\theta)$ and $c_2 = 1.0$, $\theta_{a2} = 64.64°$, $W_{a2} = 0.0291°$, $q_2 = -0.719$, and $b_2 = 0.666$ for $\sigma_{a2}(\theta)$. We see that the above double Fano function is very much successful to reproduce the overall line shape of the observed ATR spectrum. Once the second set of the parameters is determined, they can be conveniently used to discuss quantitatively the characteristics of the sharp Fano line shape. In fact, the Q factor for the sharp Fano line shape is given by $\theta_{a2}/2W_{a2}$, and we obtain $Q = \sim 1100$ for the resonance seen in Figs. 2(b) and 2(d). We note here that the double Fano resonances are commonly interpreted as due to the interference of a dark mode with two bright modes and can be well described by a model of three coupled mechanical oscillators.[41–44] According to our analysis, although not shown here, the experimental ATR spectrum presented in Figs. 2(b) and 2(d) can be well fitted to the line shape function resulting from the coupled oscillator model.

To elucidate the mechanism of appearance of the sharp Fano resonance in the present structure, we have calculated electric field distributions using a 2×2 matrix method. In the calculations, we used dielectric constants and thicknesses of the layers determined from the theoretical fit of the ATR spectrum mentioned above and assumed a p-polarized plane wave of 632.8 nm in wavelength incident on the multilayer system through the prism. Figures 3(a)–3(c) show electric field distributions obtained for three different angles of incidence, 57.11°, 64.20°, and 64.64°, respectively. In these figures, the square of the electric field amplitude normalized to that of the incident light (field enhancement factor) is plotted as a function of the position z in the structure; the z axis is normal to the interfaces and the prism/Al interface is located at $z = 0$. Note that the first and third angles chosen are the SPP excitation angle θ_{a1} and the resonance angle of the sharp Fano line shape θ_{a2}, respectively, determined from the double Fano fitting; the second angle is in between these angles.

In Figs. 3(a)–3(c), we see electric field distributions resulting from the hybridization of the SPP and PWG modes; their relative contributions vary depending on the angle of incidence. In fact, in Fig. 3(a) corresponding to the SPP resonance angle of $\theta_{a1} = 57.11°$, we see a strong contribution of the SPP excitation at the Al/SiO_2 interface, which is manifested by a strong electric field amplitude at the interface accompanied by an evanescent tail in the SiO_2 spacer layer. At this angle, the excitation of the PWG mode is weak and gives only a small bump in the Al_2O_3 waveguide. Figure 3(b) corresponding to the intermediate angle of 64.20° shows that both the SPP and PWG mode excitations contribute almost equally to the distribution; the field enhancement factor at this angle is very small because the angle is far from the SPP and PWG mode resonances. In Fig. 3(c) corresponding to $\theta_{a2} = 64.64°$, we see that the field distribution is dominated by the PWG mode excitation with an extremely high enhancement factor around the center of the waveguide. From the behaviors seen in Figs. 3(a)–3(c), it is clear that the

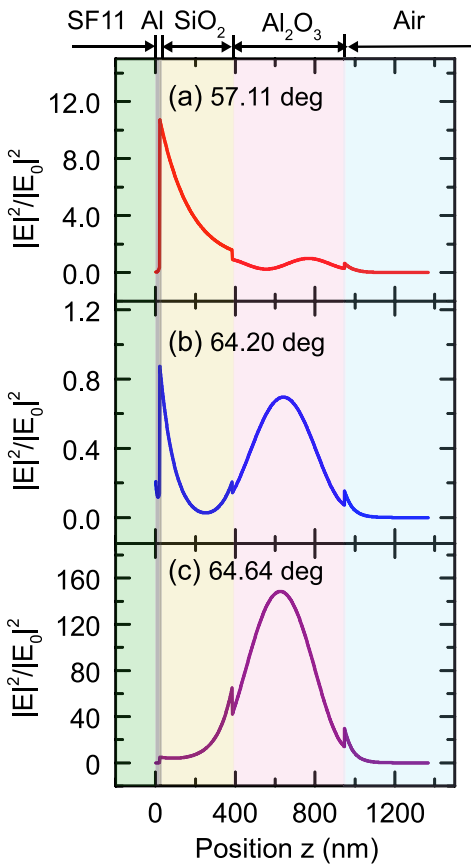

FIG. 3. Electric field distributions calculated for three different angles of incidence: (a) 57.11° ($=\theta_{a1}$), (b) 64.20°, and (c) 64.64° ($=\theta_{a2}$), respectively.

sharp Fano resonance is caused by the excitation of the PWG mode that interacts with the SPP mode. As has been shown in our theoretical paper,[23] when the angle of incidence is scanned around the resonance angle of the sharp PWG mode, the phase of the electromagnetic field associated with the PWG mode changes by a factor of π and its sign is reversed [See Fig. 5(a) in Ref. 23], while that of the SPP mode does not change appreciably because the angle is located in the tail region of the broad SPP resonance. The constructive and destructive interferences of the two modes around the PWG mode resonance thus result in the sharp asymmetric Fano line shape.

B. Fano line shape engineering

According to our EM calculations,[22–24] high-Q Fano resonances in the metal-dielectric multilayer structures have potentials to realize extremely high sensitivities in optical sensing and giant electric-field enhancements. To realize such high performances, we have to know how to engineer the Fano line shape. Our calculations demonstrated that the thickness of the spacer layer t is one of the most important parameters that determine the width W.[23,24] Physically speaking, the thickness of the spacer layer t governs the strength of coupling between the SPP and PWG modes; as t increases, the coupling becomes weaker. To generate a well-shaped Fano resonance in an ATR spectrum, the coupling has to be sufficiently small because when the coupling is too strong, the resonance splits into two separate components, not resulting in the Fano line shape; t has to be sufficiently large to generate a well-shaped Fano resonance. We found that as t increases, initially W of the Fano resonance decreases rapidly, then turns to decrease slowly, and finally approaches a minimum value for very large t values [See Fig. 8(b) in Ref. 23 and Fig. 5(e) in Ref. 24]; the Q factor, which is inversely proportional to W, thus increases in parallel with W and finally approaches a maximum value. It is very important to note here that in a real waveguide layer, the imaginary part of its dielectric constant, which reflects the loss of EM energy inside the waveguide, is normally small but is not totally zero. Our results of numerical calculations demonstrated that the minimum value of W and the maximum of Q factor are governed by the magnitude of the imaginary part; an order of magnitude increase in the imaginary part leads to roughly an order of magnitude increase (decrease) in the minimum (maximum) value of W (Q factor) [See Fig. 8(b) in Ref. 23 and Fig. 5(e) in Ref. 24].

Our EM calculations also demonstrated that the imaginary part of dielectric constant plays an important role in determining the height of the Fano resonance H, defined as $H = R_{max} - R_{min}$, with R_{max} and R_{min} being the maximum and minimum values of the reflectance around the resonance. As t increases, first H does not change appreciably, but for t larger than a threshold value, H starts to decrease very rapidly [See Fig. 8(a) in Ref. 23 and Fig. 5(d) in Ref. 24]. This means that the Fano resonance practically disappears for t values much larger than the threshold value. The threshold value was found to decrease as the imaginary part increases. Since H decreases faster than W in the region of large t, the ratio of H to W (H/W) takes a maximum value at a certain value of t. The FOM of sensitivity and FEF show almost the same t-dependence as the ratio H/W and take maximum values at a certain value of t [See Fig. 10 in Ref. 23 and Figs. 5(f) and 6(d) in Ref. 24]. This means that there exists an optimum thickness of the spacer layer, which leads to the maximum performance of the devices. It is important to note that the maximum values of the FOM and FEF are fixed by the magnitude of the imaginary part; the larger the imaginary part, the lower the maximum values. These findings suggest that in real multilayer structures, the imaginary part has to be properly estimated and the estimated value has to be used in theoretical calculations. Simulation results obtained with the unrealistic value of the imaginary part are meaningless in practical applications. As already mentioned at the beginning of Subsection III A, the imaginary part of the dielectric constant of the Al_2O_3 waveguide layer in the present samples estimated from the Winspall fitting falls in the range of 10^{-4}.

To confirm experimentally the above theoretical predictions and establish a way of engineering the Fano line shape, in particular, the width and Q factor, we prepared various samples having different spacer layer thicknesses and performed a systematic ATR study. In Figs. 4(a)–4(c), experimental Fano line shapes observed for three different samples are presented. The thicknesses of the spacer layer obtained from the Winspall fit are $t = 223$, 363, and 426 nm, respectively. The solid lines in the figures are the results of fitting to the double Fano function [Eq. (2)]. We see that the experimental line shapes are very well reproduced by the double

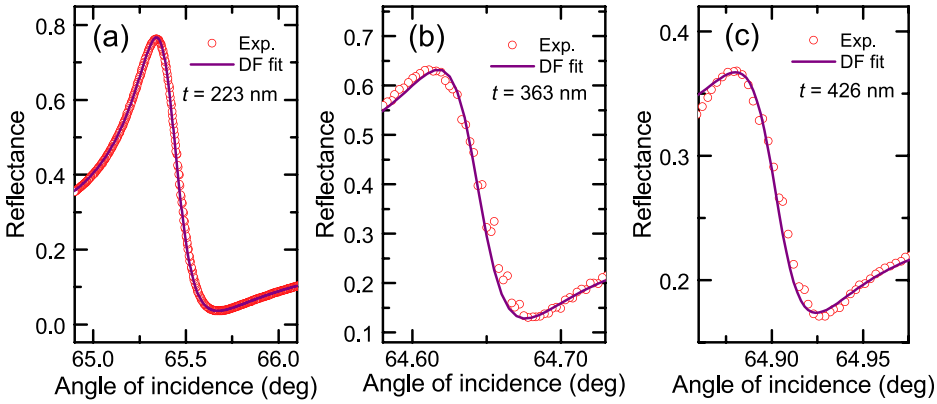

FIG. 4. Fano line shapes observed (open circles) for samples with different spacer layer thicknesses, $t = 223$ nm for (a), 363 nm for (b), and 426 nm for (c), respectively. The results of fitting to the double Fano function are presented by solid lines.

Fano fit curves. It should be noted that the scales of the ordinate and abscissa are expanded more and more in order of Figs. 4(a)–4(c). These figures demonstrate that as t increases, the width of the resonance and its height decrease, in good qualitative agreement with the theoretical predictions mentioned above. The fit to the double Fano function yields $W_{a2} = 0.1388°$, $0.0291°$, and $0.0221°$ for the three samples, respectively. We note here that the structural parameters other than t, i.e., s, d, ε_{Al}, ε_{SiO_2}, and $\varepsilon_{Al_2O_3}$, resulting from the Winspall fit, fluctuate to some extent from sample to sample. However, a comparison between the results of Winspall fitting and those of double Fano fitting indicated that W_{a2} and H are very sensitive to t and the imaginary part of $\varepsilon_{Al_2O_3}$ and less sensitive to other parameters. On the other hand, the asymmetry factor q_2 is sensitive to s and ε_{Al}, while θ_{a2} is sensitive to d and the real part of $\varepsilon_{Al_2O_3}$. W_{a2} and H are also influenced by the imaginary part of ε_{SiO_2}, but the influences are very small compared to those brought by the imaginary part of $\varepsilon_{Al_2O_3}$. In brief, the spacer layer thickness t and the imaginary part of $\varepsilon_{Al_2O_3}$ are found to be the most important parameters that determine the width W_{a2} and height H of the sharp Fano resonance in the present structure.

The results of the systematic study obtained by varying t are presented in Figs. 5(a)–5(d). In Figs. 5(a) and 5(b), experimental values of W_{a2} and Q factor are plotted as a function of t, respectively. In Figs. 5(c) and 5(d), experimental values of H and H/W_{a2} are plotted, respectively. In all these figures, theoretical curves obtained from EM calculations are also shown; a model used for the calculations is explained in detail later. Figure 5(a) demonstrates that W_{a2} decreases by approximately an order of magnitude when t increases from 200 to 450 nm. Since θ_{a2} values for various samples fall in a narrow angle region, the t-dependence of Q shown in Fig. 5(b) is mainly determined by that of W_{a2}, resulting in an order of magnitude increase in the same range of t. Note that the maximum value of Q achieved for the present sample is as high as ~1500. This Q factor is more than four times larger than that of ~350 achieved in our previous experimental work[26] and an order of magnitude larger than those of ~100 achieved by other groups for plasmonic nanostructures.[45,46] Figure 5(c) shows that H decreases monotonously as t increases. Since H decreases faster than W_{a2} for $t \gtrsim 400$ nm, the ratio H/W_{a2} takes a maximum value around $t = 370$ nm as seen in Fig. 5(d).

To obtain theoretical curves shown in Figs. 5(a)–5(d), we assumed a model structure characterized by a set of parameters: $s = 17.80$ nm and $\varepsilon_{Al} = -36.66 + i16.83$ for the Al layer, $\varepsilon_{SiO_2} = 2.125 + i1.46 \times 10^{-3}$ for the SiO_2 layer,

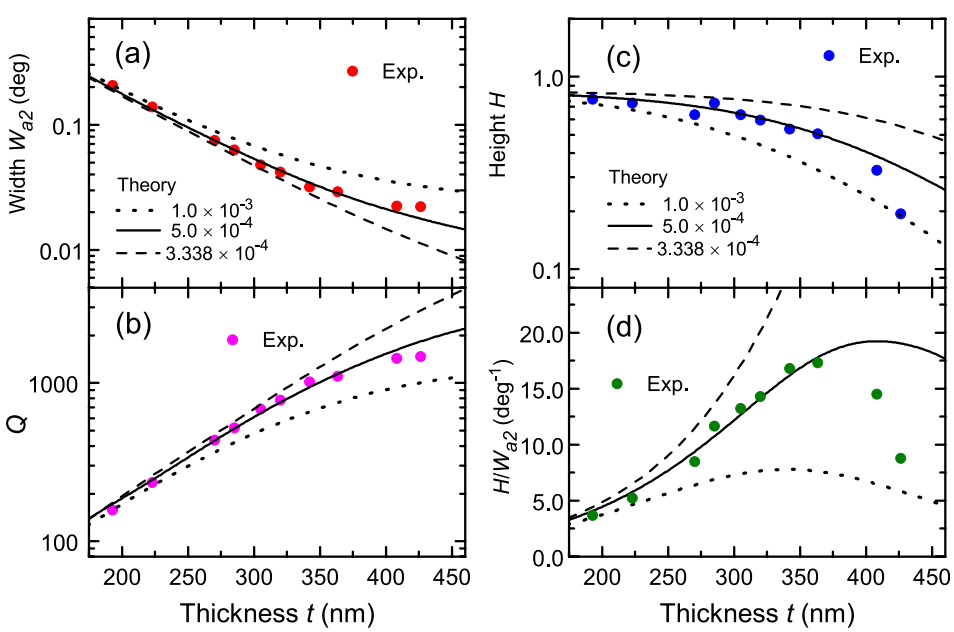

FIG. 5. Dependence of width W_{a2} (a) and Q factor (b) of the sharp Fano line shape on the spacer layer thickness t and the dependence of height H (c) and ratio H/W_{a2} (d) on t. Theoretical curves obtained from EM calculations for a model structure are also shown. The imaginary part of the dielectric constant of the Al_2O_3 waveguide layer was assumed to be $\varepsilon^{im}_{Al_2O_3} = 1.0 \times 10^{-3}$, 5.0×10^{-4}, and 3.338×10^{-4} to obtain dotted, solid, and broken curves, respectively.

and $d = 585$ nm and $\varepsilon_{Al_2O_3} = 2.786 + i\varepsilon^{im}_{Al_2O_3}$ for the Al_2O_3 layer. These parameters were determined by averaging Winspall fit parameters of different series of samples. The imaginary part of $\varepsilon_{Al_2O_3}$ was set to three different values, $\varepsilon^{im}_{Al_2O_3} = 1.0 \times 10^{-3}$, 5.0×10^{-4}, and 3.338×10^{-4}, respectively. These values can be converted into the imaginary parts of the refractive index of $\kappa = 3.0 \times 10^{-4}$, 1.5×10^{-4}, and 1.0×10^{-5}, respectively. First, assuming the above parameters and $\varepsilon^{im}_{Al_2O_3}$ values, we calculated the ATR spectra for various t. Then, we performed double Fano fitting to all the calculated spectra to obtain the values of θ_{a2} and $2W_{a2}$ as functions of t. The dotted, solid, and broken curves presented in Figs. 5(a)–5(d) correspond to the $\varepsilon^{im}_{Al_2O_3}$ values of 1.0×10^{-3}, 5.0×10^{-4}, and 3.338×10^{-4}, respectively. We see that the present experimental points of W_{a2} and the Q factor are in good agreement with the theoretical curves corresponding to $\varepsilon^{im}_{Al_2O_3} = 5.0 \times 10^{-4}$. A close comparison between the theoretical curves reveals that for small t values, the difference in $\varepsilon^{im}_{Al_2O_3}$ does not lead to large differences in W_{a2} and Q. However, as t increases, the difference between the curves becomes larger, and for $t \gtrsim 350$ nm, the differences are considerably large. These behaviors of the theoretical curves can be explained physically in the following way. In the region of small t, the coupling between the SPP and PWG modes is relatively strong, and it is the coupling strength that determines the width of the Fano resonance W_{a2}. Therefore, W_{a2} and Q are governed by the coupling strength rather than by the loss in the waveguide represented by $\varepsilon^{im}_{Al_2O_3}$. On the other hand, in the region of large t, the coupling becomes weak and the loss in the waveguide plays a major role in determining W_{a2} and Q. In the intermediate region of t, W_{a2} and Q are determined by the interplay of the coupling strength and the loss.

In Fig. 5(c), we see that for $t \lesssim 350$ nm, the experimental points of H are located very close to the theoretical curve corresponding to $\varepsilon^{im}_{Al_2O_3} = 5.0 \times 10^{-4}$, while for $t \gtrsim 350$ nm, the points deviate from the curve and tend to approach the curve corresponding to $\varepsilon^{im}_{Al_2O_3} = 1.0 \times 10^{-3}$. The same behavior of the experimental points of H/W_{a2} is seen in Fig. 5(d). The reason for the deviation of the experimental points from the theoretical curves of $\varepsilon^{im}_{Al_2O_3} = 5.0 \times 10^{-4}$ is not well understood at present; light scattering caused by the surface roughness at the waveguide surface, which is not included in the EM calculations, may be one of the reasons. Nevertheless, the present experimental data clearly demonstrate the existence of a maximum in H/W_{a2}, in good agreement with the theoretical result mentioned above. It is now very clear that the discussion of the Fano line shape that does not take into account the influence of the nonzero imaginary part is meaningless, in particular, in the region of large t. Very recently, Zheng *et al.*[29] reported an extremely high theoretical value of $Q = 63\,895.4$ for a multilayer structure consisting of an Au layer, a SiO_2 layer, and a ZrO_2 layer surrounded by water. This high Q value is unrealistic because they estimated it from an EM calculation neglecting the imaginary part of the dielectric constant of the ZrO_2 waveguide layer.

Finally, we note that the sharp Fano resonances in the metal-dielectric multilayer structures are very much promising in developing high-performance optical devices such as sensors, optical switches, and platforms of enhanced spectroscopies. In biosensing, for instance, surface plasmon resonance (SPR) sensors have been widely used. In the conventional SPR biosensor, it is common to functionalize metallic surfaces to capture desired biomolecules and monitor changes in the SPP ATR dips caused by the capture of the biomolecules. The metal-dielectric multilayer structure can be used in exactly the same manner as the SPR biosensor, when the outer surface of the waveguide layer is functionalized and the biomolecules are captured thereon. According to our previous numerical analyses,[22–24] when the change in the intensity of the reflected light is monitored, sharper Fano resonances are expected to lead larger FOM of sensitivity. Although the ultimate FOM of sensitivity is determined by the material parameters, in particular, the imaginary part of dielectric constant of the waveguide, the FOM of sensitivity for an optimized structure can be enhanced by several orders of magnitude compared to that of the conventional SPR biosensor. Highly enhanced electric fields generated at the waveguide surface under the Fano resonance condition can also be used to monitor enhanced Raman and fluorescence signals from attached biomolecules.[23,24]

IV. CONCLUSIONS

We have demonstrated that the multilayer samples, consisting of an Al layer, a SiO_2 spacer layer, and an Al_2O_3 waveguide layer, exhibit high-Q Fano resonances in the angle-scan ATR spectra measured in the Kretschmann configuration. The Fano resonances originate from the coupling between the SPP mode at the Al/SiO_2 interface and the PWG mode supported by the Al_2O_3 waveguide. The sharp Fano resonance was observed on the background of highly asymmetric and broad resonance corresponding to the excitation of the SPP mode at the Al/SiO_2 interface. We showed that the asymmetric line shape of the SPP resonance can be well reproduced by the generalized Fano function derived by Gallinet and Martin.[38,39] Furthermore, we showed that the sharp Fano line shape can be well reproduced by the generalized double Fano function, which is expressed as a product of two generalized Fano functions. The dependence of the Fano line shape on the spacer layer thickness was systematically studied and compared with theoretical results. The width of the Fano resonance was found to decrease monotonously as the spacer layer thickness increases, leading to the increase in the Q factor. The Q factor achieved in the present work is as high as $\sim$1500. A comparison between the experiment and theory reveals that not only the spacer layer thickness, which governs the coupling strength, but also the imaginary part of the dielectric constant related to the loss in the waveguide play an important role in determining the width and height of the Fano resonance.

In this work, we concentrated on sharpening the Fano resonance to achieve high Q factors, varying the thickness of the SiO_2 spacer layer, while fixing that of the Al_2O_3 waveguide layer. Further detailed studies are still required to achieve high sensing sensitivities and high field enhancement factors. A careful optimization of the structure is necessary, in particular, regarding the position of the sharp Fano resonance, which can be controlled by the thickness of the

Al_2O_3 layer. Such an optimization is underway in our group, and results will be published elsewhere. In view of good plasmonic properties of Al in the UV region, the results presented in this paper may pave the way for realizing the Fano resonance and developing its applications in the UV spectral region.

ACKNOWLEDGMENTS

This work was supported by JSPS KAKENHI Grant No. 16K04979.

[1]H. P. Chiang, H. T. Yeh, C. M. Chen, J. C. Wu, S. Y. Su, R. Chang, Y. J. Wu, D. P. Tsai, S. U. Jen, and P. T. Leung, "Surface plasmon resonance monitoring of temperature via phase measurement," Opt. Commun. **241**, 409 (2004).
[2]S. Lal, S. Link, and N. J. Halas, "Nano-optics from sensing to waveguiding," Nat. Photonics **1**, 641 (2007).
[3]N. I. Zheludev and Y. S. Kivshar, "From metamaterials to metadevices," Nat. Mater. **11**, 917 (2012).
[4]P. C. Wu, W. L. Hsu, W. T. Chen, Y. W. Huang, C. Y. Liao, N. I. Zheludev, G. Sun, and D. P. Tsai, "Plasmon coupling in vertical split-ring resonator metamolecules," Sci. Rep. **5**, 9726 (2015).
[5]P. C. Wu, C. Y. Liao, J. W. Chen, and D. P. Tsai, "Isotropic absorption and sensor of vertical split-ring resonator," Adv. Opt. Mater. **5**, 1600581 (2017).
[6]A. E. Miroshnichenko, S. Flach, and Y. S. Kivshar, "Fano resonances in nanoscale structures," Rev. Mod. Phys. **82**, 2257 (2010).
[7]B. Luk'yanchuk, N. I. Zheludev, S. A. Maier, N. J. Halas, P. Nordlander, H. Giessen, and C. T. Chong, "The Fano resonance in plasmonic nanostructures and metamaterials," Nat. Mater. **9**, 707 (2010).
[8]N. J. Halas, S. Lal, W.-S. Chang, S. Link, and P. Nordlander, "Plasmons in strongly coupled metallic nanostructures," Chem. Rev. **111**, 3913 (2011).
[9]A. B. Khanikaev, C. Wu, and G. Shvets, "Fano-resonant metamaterials and their applications," Nanophotonics **2**, 247 (2013).
[10]M. Rahmani, B. Luk'yanchuk, and M. Hong, "Fano resonance in novel plasmonic nanostructures," Laser Photonics Rev. **7**, 329 (2013).
[11]M. F. Limonov, M. V. Rybin, A. N. Poddubny, and Y. S. Kivshar, "Fano resonances in photonics," Nat. Photonics **11**, 543 (2017).
[12]A. Christ, Y. Ekinci, H. H. Solak, N. A. Gippius, S. G. Tikhodeev, and O. J. F. Martin, "Controlling the Fano interference in a plasmonic lattice," Phys. Rev. B **76**, 201405(R) (2007).
[13]J. B. Lassister, H. Sobhani, J. A. Fan, J. Kundu, F. Capasso, P. Nordlander, and N. J. Halas, "Fano resonances in plasmonic nanoclusters: Geometrical and chemical tunability," Nano Lett. **10**, 3184 (2010).
[14]J. B. Lassister, H. Sobhani, M. W. M. W. S. Knight, P. Nordlander, and N. J. Halas, "Designing and deconstructing the Fano lineshape in plasmonic nanoclusters," Nano Lett. **12**, 1058 (2012).
[15]S. N. Sheikholeslami, A. Garcia-Extarri, and J. A. Dionne, "Controlling the interplay of electronic and magnetic modes via Fano-like plasmon resonances," Nano Lett. **11**, 3927 (2011).
[16]W.-S. Chang, J. B. Lassister, P. Swanglap, H. Sobhani, S. Khatua, P. Nordlander, N. J. Halas, and S. Link, "A plasmonic Fano switch," Nano Lett. **12**, 4977 (2012).
[17]Z.-J. Yang, Q.-Q. Wang, and H.-Q. Lin, "Tunable two types of Fano resonances in metal-dielectric core-shell nanoparticle clusters," Appl. Phys. Lett. **103**, 111115 (2013).
[18]Y. Sonnerfraud, N. Verellen, H. Sobhani, G. A. E. Vandenbosch, V. V. Moshchalkov, P. V. Dorpe, P. Nordlander, and S. A. Maier, "Experimental realization of subradiant, superradiant, and Fano resonances in ring/disk plasmonic nanocavities," ACS Nano **4**, 1664 (2010).
[19]Y. H. Fu, J. B. Zhang, Y. F. Yu, and B. Luk'yanchuk, "Generating and manipulating higher order Fano resonances in dual-disk ring plasmonic nanostructures," ACS Nano **6**, 5130 (2012).
[20]J. Li, T. Liu, H. Zheng, J. Dong, E. He, W. Gao, Q. Han, C. Wang, and Y. Wu, "Higher-order Fano resonances and electric field enhancements in disk-ring plasmonic nanostructures with double symmetry breaking," Plasmonics **9**, 1439 (2014).
[21]J. Qi, C. Z. J. Chen, Y. Li, W. Qiang, J. Xu, and Q. Sun, "Independently tunable double Fano resonances in asymmetric MIM waveguide structure," Opt. Express **22**, 14688 (2014).
[22]S. Hayashi, D. V. Nesterenko, and Z. Sekkat, "Fano resonance and plasmon-induced transparency in waveguide-coupled surface plasmon resonance sensors," Appl. Phys. Express **8**, 022201 (2015).
[23]S. Hayashi, D. V. Nesterenko, and Z. Sekkat, "Waveguide-coupled surface plasmon resonance sensor structures: Fano lineshape engineering for ultrahigh-resolution sensing," J. Phys. D: Appl. Phys. **48**, 325303 (2015).
[24]D. V. Nesterenko, S. Hayashi, and Z. Sekkat, "Extremely narrow resonances, giant sensitivity and field enhancement in low-loss waveguide sensors," J. Opt. **18**, 065004 (2016).
[25]Z. Sekkat, S. Hayashi, D. V. Nesterenko, A. Rahmouni, S. Refki, H. Ishitobi, Y. Inouye, and S. Kawata, "Plasmonic coupled modes in metal-dielectric multilayer structures: Fano resonance and giant field enhancement," Opt. Express **24**, 20080 (2016).
[26]S. Hayashi, D. V. Nesterenko, A. Rahmouni, and Z. Sekkat, "Observation of Fano line shapes arising from coupling between surface plasmon polariton and waveguide modes," Appl. Phys. Lett. **108**, 051101 (2016).
[27]S. Hayashi, D. V. Nesterenko, A. Rahmouni, H. Ishitobi, Y. Inouye, and S. Kawata, "Light-tunable Fano resonance in metal-dielectric multilayer structures," Sci. Rep. **6**, 33144 (2016).
[28]S. Hayashi, D. V. Nesterenko, A. Rahmouni, and Z. Sekkat, "Polarization effects in light-tunable Fano resonance in metal-dielectric multilayer structures," Phys. Rev. B **95**, 165402 (2017).
[29]G. Zheng, J. Cong, L. Xu, and J. Wang, "High-resolution surface plasmon resonance sensor with Fano resonance in waveguide-coupled multilayer structures," Appl. Phys. Express **10**, 042202 (2017).
[30]W. L. Barnes and J. R. Sambles, "Thin Langmuir-Blodgett films studied using surface plasmon-polaritons," Surf. Sci. **183**, 189 (1987).
[31]A. Shinya, Y. Okuno, M. Fukui, and Y. Shintani, "Wavelength dependence of the dielectric constant of thermally evaporated aluminum films," Surf. Sci. **371**, 149 (1997).
[32]D. Gérard and S. K. Gray, "Aluminium plasmonics," J. Phys. D: Appl. Phys. **48**, 184001 (2015).
[33]M. F. Cardinal, E. V. Ende, R. A. Hackler, M. O. McAnally, P. C. Stair, G. C. Schatz, and R. P. Van Duyne, "Expanding applications of SERS through versatile nanomaterials engineering," Chem. Soc. Rev. **46**, 3886 (2017).
[34]M. N. Polyanskiy, see http://refractivindex.info/ for Refractive index database, 2015.
[35]C. Langhammer, M. Schwind, B. Kasemo, and I. Zorić, "Localized surface plasmon resonances in aluminum nanodisks," Nano Lett. **8**, 1461 (2008).
[36]E. Kretschmann, "Die Bestimmung optischer Konstanten von Metallen durch Anregung von Oberflächenplasmaschwingungen," Z. Phys. **241**, 313 (1971).
[37]H. Raether, *Surface Plasmons on Smooth and Rough Surfaces and on Gratings*, Springer Tracts in Modern Physics Vol. 111 (Springer-Verlag, 1988).
[38]B. Gallinet and O. J. F. Martin, "*Ab initio* theory of Fano resonances in plasmonic nanostructures and metamaterials," Phys. Rev. B **83**, 235427 (2011).
[39]B. Gallinet and O. J. F. Martin, "Influence of electromagnetic interactions on the line shape of plasmonic Fano resonances," ACS Nano **5**, 8999 (2011).
[40]U. Fano, "Effects of configuration interaction on intensities and phase shifts," Phys. Rev. **124**, 1866 (1961).
[41]K. Ueda, "Spectral line shapes of autoionizing Rydberg series," Phys. Rev. A **35**, 2484 (1987).
[42]Z. Bai, C. Hang, and G. Huang, "Classical analogs of double electromagnetically induced transparency," Opt. Commun. **291**, 253 (2013).
[43]Y. U. Lee, E. Y. Choi, E. S. Kim, J. H. Woo, B. Kang, J. Kim, B. C. Park, T. Y. Hong, J. H. Kim, and J. W. Wu, "Double Fano resonances in a composite metamaterial possessing tripod plasmonic resonances," J. Opt. **17**, 025103 (2015).
[44]S. Yin, X. Lu, N. Xu, S. Wang, Y. E, X. Pan, X. Xu, H. Liu, L. Chen, W. Zhang, and L. Wang, "Spoof surface plasmon polaritons in terahertz transmission through subwavelength hole arrays analyzed by coupled oscillator model," Sci. Rep. **5**, 16440 (2015).
[45]W. Cao, R. Singh, I. A. I. Al-Naib, M. He, A. J. Taylar, and W. Zhang, "Low-loss ultra-high-Q dark mode plasmonic Fano metamaterials," Opt. Lett. **37**, 3366 (2012).
[46]P. Gu, M. Wan, Q. Shen, X. He, Z. Chen, P. Zhan, and Z. Wang, "Experimental observation of sharp cavity plasmon resonances in dielectric-metal core-shell resonator," Appl. Phys. Lett. **107**, 141908 (2015).